Clim Dyn (2007) 29:501–520
DOI 10.1007/s00382-007-0244-y

Impact of different convective cloud schemes on the simulation of the tropical seasonal cycle in a coupled ocean–atmosphere model

P. Braconnot · F. Hourdin · S. Bony · J. L. Dufresne · J. Y. Grandpeix · O. Marti

Received: 8 June 2006 / Accepted: 28 February 2007 / Published online: 11 April 2007

Abstract The simulation of the mean seasonal cycle of sea surface temperature (SST) remains a challenge for coupled ocean–atmosphere general circulation models (OAGCMs). Here we investigate how the numerical representation of clouds and convection affects the simulation of the seasonal variations of tropical SST. For this purpose, we compare simulations performed with two versions of the same OAGCM differing only by their convection and cloud schemes. Most of the atmospheric temperature and precipitation differences between the two simulations reflect differences found in atmosphere-alone simulations. They affect the ocean interior down to 1,000 m. Substantial differences are found between the two coupled simulations in the seasonal march of the Intertropical Convergence Zone in the eastern part of the Pacific and Atlantic basins, where the equatorial upwelling develops. The results confirm that the distribution of atmospheric convection between ocean and land during the American and African boreal summer monsoons plays a key role in maintaining a cross equatorial flow and a strong windstress along the equator, and thereby the equatorial upwelling. Feedbacks between convection, large-scale circulation, SST and clouds are highlighted from the differences between the two simulations. In one case, these feedbacks maintain the ITCZ in a quite realistic position, whereas in the other case the ITCZ is located too far south close to the equator.

P. Braconnot (✉) · O. Marti
IPSL/LSCE, unité mixte CEA-CNRS-UVSQ,
Bât.712, Orme des Merisiers,
91191 Gif-sur-Yvette Cedex, France
e-mail: pascale.Braconnot@cea.fr

F. Hourdin · S. Bony · J. L. Dufresne · J. Y. Grandpeix
IPSL/LMD, Unité mixte CNRS-Ecole
Polytechnique-ENS-UPMC, case 99,
4 Place Jussieu, 75252 Paris cedex 05, France

1 Introduction

The representation of clouds and atmospheric convection has been emphasized as a critical issue for the simulation of the current climate in various coupled ocean–atmosphere models (IPCC 2001). In particular coupled models have a tendency to produce a warm bias in the eastern Pacific and Atlantic oceans where the equatorial upwelling develops from the eastern boundary (Latif et al. 2001; Davey et al. 2002). The representation of the seasonal cycle of sea surface temperature (SST), such as the representation of the seasonal evolution of the equatorial upwelling in the eastern Pacific, remains a challenge for coupled simulations. Our understanding of this mode of variability of the coupled ocean–atmosphere system (Wang 1994) suggests that the simulation of this variability dependens on the numerical representation of clouds and convection. Indeed, the existence of the cold tongue along the equator is an annual response of the climate system to the semi-annual forcing of incoming solar radiation at the top of the atmosphere in this region. It results from complex atmosphere–ocean interaction (Wang 1994). Two modes have been identified so far that shape the seasonal evolution of SST in this region (Wang 1994; Nigam and Chao 1996). The first one is related to the monsoon circulation that converges in central America. This mode represents the tropical part of a global response of the atmosphere–land–ocean system to the differential insolation between the

northern and southern hemisphere (Wang 1994). The second mode results from large-scale air–sea interactions, and involves the relationship between SST gradients and wind, the latent heat flux and the presence of a stratocumulus deck in the subsiding regions of the east Pacific. Several studies have shown that the interactions between low-level moisture, stratocumulus deck and cloud radiative properties contribute to the maintenance of the cold tongue (Ma et al. 1996; Yu and Mechoso 1999; Gordon et al. 2000).

In that vein, we investigate how atmospheric convection and clouds impact the large-scale atmospheric and oceanic circulation in the tropical regions, using two versions of a coupled ocean–atmosphere model differing only by the parameterisation of convective clouds. The two simulations show substantial differences in the tropical circulation. The objective of the paper is thus to highlight differences in the adjustment of the ocean–atmosphere system to convective cloud schemes, and to show how the interaction between clouds, convection and the large-scale circulation affects the characteristics of the mean climate and of the mean seasonal cycle in the tropics. A particular emphasis is put on the eastern part of the equatorial Pacific and Atlantic oceans. The reason is that the analysis of the two simulations allows us to identify how the feedbacks between the large-scale atmospheric dynamics and the oceanic circulation shape the evolution of the seasonal cycle of precipitation and temperature in these regions.

We use the most recent version of the Institut Pierre Simon Laplace (IPSL, Paris) coupled ocean–atmosphere model (Marti et al. 2005). A major change in the atmospheric component, LMDZ, with respect to the previous version comes from the replacement of the convection scheme of Tiedtke (1989), originally implemented in the LMDZ atmospheric model (Li 1999), by the Emanuel (1993)'s scheme. This change has significantly improved the large-scale distribution of tropical precipitation in atmosphere-alone simulations (Hourdin et al. 2006). The Inter Tropical Convergence zone (ITCZ) is now less confined along the equator, and precipitations are in better agreement with observations over the Amazonian basin. The rate of warming and moistening of the atmospheric column by convection is also at the origin of substantial differences in the simulation of the land–sea contrast in convection and of the large-scale tropical atmospheric circulation. Our purpose here is to analyse how these differences impact the simulated climate when the atmosphere is coupled to the ocean.

The remainder of the manuscript is organized as follows. Section 2 gives a short description of the coupled model, with emphasis on the convection and cloud schemes, and presents the major characteristics of the simulations. Differences in the tropical circulation simulated by the two convection schemes are analysed in Sect. 3. Section 4 discusses differences in the timing and in the amplitude of the tropical seasonal cycle. The mechanisms responsible for the differences in the seasonal march of the ITCZ in the eastern equatorial Pacific and Atlantic oceans are discussed in Sect. 5. Comparison with atmosphere alone simulations helps us to understand the role of the interactions between convection and the large-scale circulation in the tropics. The conclusion is given in Sect. 6.

2 Model and simulations

2.1 Model description

Simulations were performed with the most recent version of the coupled model developed at IPSL (Marti et al. 2005). IPSL_CM4 couples the grid point atmospheric general circulation model LMDZ (Hourdin et al. 2006) developed at Laboratoire de Météorologie Dynamique (LMD, France) to the oceanic general circulation model ORCA (Madec et al. 1998) developed at the Laboratoire d'Océanographie et du Climat (LOCEAN, ex LODYC, France). On the continent, the land surface scheme ORCHIDEE (Krinner et al. 2005) is coupled to the atmospheric model. Only the thermodynamic component of ORCHIDEE is active in the simulations presented here. The closure of the water budget with the ocean is achieved thanks to a river routing scheme implemented in the land surface model. A sea-ice model (Fichefet and Maqueda 1997), which computes ice thermodynamics and dynamics, is included in the ocean model. The ocean and atmospheric models exchange surface temperature, sea-ice cover, momentum, heat and fresh water fluxes once a day, using the OASIS coupler (Terray et al. 1995) developed at CERFACS (France). None of these fluxes is corrected.

Compared to previous versions of the IPSL model (Braconnot et al. 2000; Dufresne et al. 2002), the coupling scheme was revisited to ensure both global and local conservations of momentum, heat and fresh water fluxes at the air–sea interface (Marti et al. 2005). Following some of the ideas implemented in previous model versions (Dufresne and Grandpeix 1996; Braconnot 1998), an interface model was implemented in the atmospheric model. Each atmospheric column is interfaced with up to four different surface types: ocean, land, sea-ice, and land ice. Surface fluxes are computed according to the surface characteristics (roughness length, stability etc.).

In its present configuration, the model is run at medium resolution. The atmospheric grid is regular, with a resolution of 3.75° in longitude, 2.5° in latitude, and 19 vertical levels. The ocean model grid has approximately 2 degrees resolution (0.5 degrees near the equator) with 182 points in longitude, 149 points in latitude and 31 1evels in the ocean.

2.2 Convection and cloud scheme

The coupled model is run either with the Emanuel's or the Tiedtke's convection scheme. These schemes are used to represent both deep and shallow convections, whether they give a unique (Emanuel) or separate (Tiedtke) treatment to these two processes. These schemes both belong to the category of ''mass flux schemes''. They parameterize the convective mass fluxes as well as the induced motions in the environmental air. In the Tiedtke's (1989) scheme, only one convective cloud is considered, comprising one single saturated updraught. Entrainment and detrainment between the cloud and the environment can take place at any level between the free convection level and the free sinking level. There is also one single downdraught extending from the free sinking level to the cloud base. The mass flux at the top of the downdraught is a constant fraction (here 0.3) of the convective mass flux at cloud base. This downdraught is assumed to be saturated and is kept at saturation by evaporating precipitation. The version of the Tiedtke's scheme used here is close to its original formulation and uses a closure in moisture convergence. Triggering is a function of the buoyancy of lifted parcels at the first grid level above condensation level.

In the Emanuel's scheme, the backbone of the convective systems is an adiabatic ascent originating from some low-level layer and ending at their level of neutral buoyancy. Shedding from these adiabatic ascents yields, at each level, a set of draughts, which are mixtures of adiabatic ascent air (from which some precipitation is removed) and environmental air. These mixed draughts move adiabatically up or down to levels where, after further removal of precipitation and evaporation of cloud water, they are at rest at their new levels of neutral buoyancy. In addition to those buoyancy-sorted saturated draughts, unsaturated downdraughts are parameterized as a single entraining plume of constant fractional area (here 1% of the grid cell) driven by the evaporation of precipitation. The version of the Emanuel's scheme used here is very similar to Emanuel (1993). Closure and triggering take into account both tropospheric instability and convective inhibition. Our version differs from the original one in the removal of most explicit grid dependencies.

The cloud scheme describes the subgrid-scale distribution of total water by a generalized log-normal distribution, whose variance and skewness are diagnosed, and that uses zero as the lower bound of the distribution. For non-convective clouds, the normalised width of the probability distribution function is imposed as an increasing function of height, following the vertical profile of total water and of saturated specific humidity (Hourdin et al. 2006). The non-convective clouds are exactly the same whatever the convection scheme used. Clouds associated with cumulus convection are predicted differently depending on the convection scheme used in the GCM. When using the Emanuel's scheme, the cloud scheme is coupled to the convection scheme by diagnosing the variance and the skewness of the total water distribution from the vertical profile of in-cloud water content predicted by the convection scheme and from the degree of saturation of the large-scale environment (Bony and Emanuel 2001). In the case of the Tiedtke's scheme, an homogeneous cloud fraction is assumed between cloud base and cloud top, that is a function of the vertically integrated moistening tendency predicted by the Tiedtke's convection scheme (Hourdin et al. 2006).

Cloud microphysical properties are computed as described by Bony and Emanuel (2001, Table 2 for water clouds and case ''ICE-OPT'' of Table 3 for ice clouds). The vertical overlap of cloud layers is assumed to be maximum-random. A more complete description of these schemes can be found in Hourdin et al. (2006).

2.3 Simulations

Two simulations have been performed with the coupled model: one using the Tiedtke convection scheme and associate cloud scheme (TI) and one using the Emanual convection scheme and associate cloud scheme (KE). Both versions of the model are equivalent from a global energetic point of view. The coupled model is equilibrated and long-term integrations can be performed without using any flux correction at the air–sea interface.

The simulation with the Emanuel's scheme, referred to as KE, corresponds to the reference version of the IPSL model that has been used for the production of IPCC AR4 scenarios (Dufresne et al. 2005; Swingedouw et al. 2006). This simulation will then be considered as the reference. It is a 500-year-long simulation. Over this period, and after the first 10 years of initial adjustment between atmosphere and ocean, the model drift in global mean surface temperature is less than 0.02°C/century. The simulation is stable with a global mean 2 m air temperature of 14°C that presents low frequency variability of about 0.1–0.2°C around this mean. In the following, we will consider a mean seasonal cycle computed from the last 200 years of the simulation.

The simulation with the Tiedtke scheme (TI) was run for 300 years. The initial state and the spin up strategy is the same as for KE. The initial adjustment drives the model in a warmer state than KE (the global mean 2 m air temperature is 15.7°C), mainly in high latitudes and over land. After the initial adjustment, the model drift is negligible, but larger than for the KE simulation (0.05°C/century). We consider the last 150 years of the simulation in the remainder of this manuscript. When needed, the results are

be compared with the atmosphere-alone simulations presented by Hourdin et al. (2006).

2.4 Datasets used for model evaluation

Several datasets are used to evaluate the performance of the model. In all cases we only consider the mean monthly climatology. SSTs are compared to Reynolds' (1988) climatology. For the interior ocean, we consider Levitus (1982) data. Precitation are compared to the CMAP dataset (Xie and Arkin 1996), which merges raingauges data over land and satellite observations over the ocean. Wind stress comes from a combination of ERS1–2 scatterometer-derived wind stresses (Bentamy et al. 1996) and TAO-Wind stresses (Menkes et al. 1998). ERS 1–2 for the 1993–1998 period were obtained from IFREMER/CERSAT (http://www.ifremer.fr/cersat). Details about the procedure used to combine these datasets can be found in Menkes et al. (1998). Several other products derived from satellite observation are used. They include ERBE estimate of the radiative fluxes at the top of the atmosphere (Barkstrom 1984), and ISCCP data for the cloud cover (Rossow and Schiffer 1999). We also consider NCEP (Kalnay et al. 1996) and ERA40 (Uppala et al. 2005) reanalyses, mostly for large-scale pressure, vertical velocity and the three dimensional structure of the atmosphere.

2.5 Simulated climate: global characteristics

Figure 1 shows the difference between the simulated annual mean SST and the Levitus (1982)'s climatology for the two simulations. The large-scale patterns of the SST field are successfully captured by the two model versions in most places.

The main shortcoming of the reference simulation (KE) is the cold bias at middle latitudes both in the Atlantic and Pacific oceans (Fig. 1a). Locally, this bias reaches 6°C in the North Atlantic, which results from the conjunction of a southward shift of the north Atlantic drift and the advection of cold water from the Gin (Groendland-Islande-Nordic seas) and the Labrador seas. It has been attributed to a lack of deep-water formation in the Labrador Sea (Swingedouw et al. 2005), caused by an excessive fresh water input over the North Atlantic, the Nordic seas and the southern part of

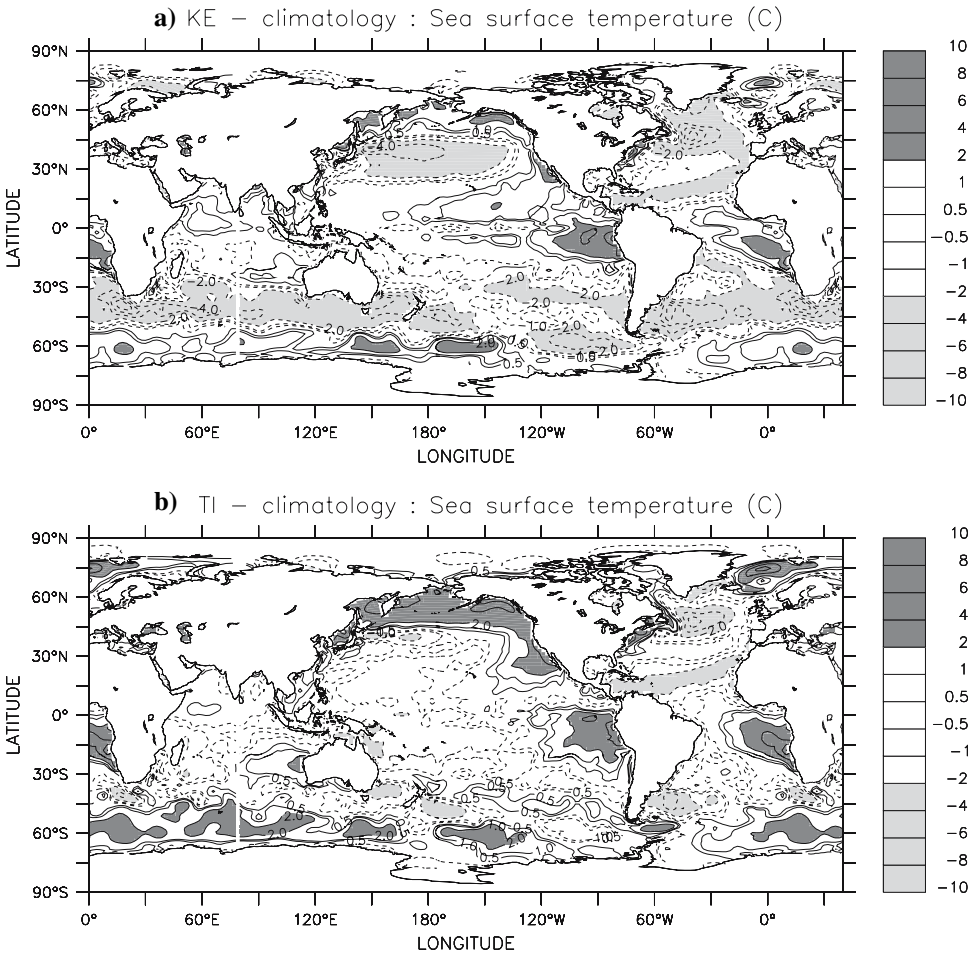

Fig. 1 Annual mean sea surface temperature difference (°C) with Levitus (1982) climatology for **a** KE and **b** TI. Values larger (*lower*) than 2°C (–2°C) are *dark* (*light*) *shaded*. *Dashed* (*solid*) *lines* stand for negative (positive) values. Isolines are plotted every 0.5°C from 0 to +/1 1, and every 2°C from ±2 to ±10°C

Greenland. A thin halocline at the surface reduces the local buoyancy of surface waters, and thus ocean convection. Note that the equatorward shift of the mid-latitude storm-tracks is already present in atmosphere alone simulations. This shift is amplified when the atmospheric model is coupled to the ocean and leads to the mid latitude cold SSTs in both hemispheres, but reduces when refining horizontal resolution (not shown).

This cold bias is not as large in the TI simulation (Fig. 1b). On the contrary, surface waters are too warm along the margin of sea-ice in the southern hemisphere and in the northern part of the Pacific ocean. The root mean square differences (rms) between the simulated map and Reynold's (1988) observations suggest that TI better reproduces global SST with a global rms of 1.4°C against 1.7°C for KE. When the rms is computed over the tropical regions (30°S–30°N), the rms is 1.5°C for TI and 1.2°C for KE. This suggests that model biases are primarily located in mid-latitudes in KE, whereas they occur at most latitudes in TI.

The major differences between the two coupled simulations and observations follow the differences highlighted in atmosphere-alone simulations (Hourdin et al. 2006). For example, Fig. 2a shows that in KE the zonal mean tem-

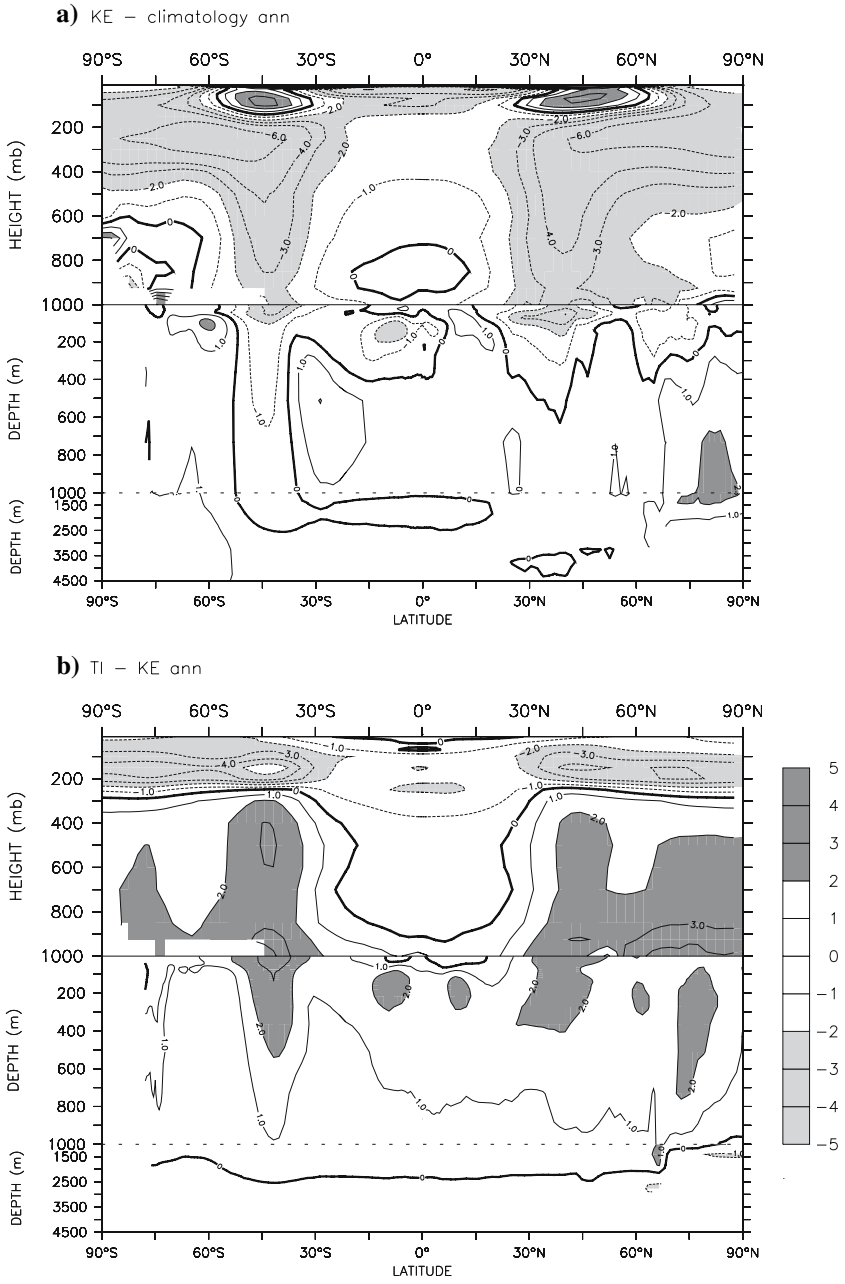

Fig. 2 Annual mean atmosphere and ocean temperature (°C), zonally averaged and plotted as a function of latitude and depth, **a** difference between KE and climatology, **b** difference between TI and KE. Note that the upper 1,000 m of the ocean are expanded. Values larger (lower) than 2°C (–2°C) are *dark* (*light*) *shaded*

perature presents a cold bias of up to 8°C at about 200 hPa. This pattern was attributed to an overestimation of the moisture content at these levels and is amplified by the coupling with the ocean. Differences in the atmosphere have their counterpart in the ocean. The KE simulation presents a slight cold bias down to 400 m in the ocean around 30°N and 40°S, consistent with the cold atmospheric bias (Fig. 2a). Elsewhere in the ocean, the departure from climatology doesn't exceed 2°C, except at high latitudes, where the warm bias at depth reflects the lack of deep-water formation.

Figure 2b also reveals that in middle and high latitudes, the TI simulation is associated with even colder conditions in the upper troposphere and lower stratosphere and warmer conditions in the lower and middle troposphere than the KE simulation. Hourdin et al (2006) show that this is due to additional humidity from ''mid-level'' convection, which results in a larger cooling to space in TI. The TI simulation is also characterized by warmer water in the upper 1,000 m of the ocean with maximum value in the two regions of intermediate water formation noted above. It is less satisfactory at depth where 1°C warmer than observed water is found down to 1,000 m.

The equator-to-pole differences in the three-dimensional structure of temperature in the ocean and atmosphere are associated with differences in the equator to pole heat transport by the oceanic and atmospheric circulations. The northward total heat transport is larger in KE than in TI, up to 1PW at 20°N, and better matches estimates derived from satellite observations and reanalyses (Trenberth and Salomon 1994).

3 Large scale features in the tropics

3.1 Large scale features of the simulated climate compared with observations

The model performs well in the tropics. In KE, errors are less than 0.5°C over most of the basins (Fig. 1a). The exception is at the eastern side of the equatorial Pacific and Atlantic where the warm bias indicates that the ocean cold tongue is not well located along the coast. This is a typical bias of coupled models, especially with the relatively coarse resolution we are using here (Latif et al. 2001). The equatorial section of annual mean temperature plotted as a function of depth (Fig. 3) shows that the vertical temperature gradient is more diffuse than in observations. However, the shape of the thermocline presents an east–west gradient in agreement with observations both in the Pacific and Atlantic oceans. In the latter, warm surface waters accumulate in the upper ocean in the eastern part of the Gulf of Guinea and the upwelling is shifted to the west. The surface ocean temperatures as well as the east–west temperature gradient at depth are also satisfactorily reproduced in KE in the Indian Ocean (Fig. 3b).

Figures 1 and 3b, c shows that TI is slightly warmer than KE in the eastern Pacific and colder over the warm pool. As a result, the east–west SST contrast is reduced by about 1.4°C in TI compared to KE across the Pacific. The difference between the two simulations is even larger in the ocean interior (Fig. 3). For example, the 14°C isotherm depth is located about 100 m deeper in the eastern part of the Pacific Ocean, suggesting that the upwelling is not strong enough. In the Atlantic, TI produces a flat thermocline across the basin. This bias leads to a reversal of the temperature gradient at the surface compared to observation. Also the temperature gradients are reversed across the Indian ocean in the upper 200 m, with warmer water in the eastern part. This comparison shows that the thermocline depth is on average deeper in TI than in KE, which suggests that the local thermal inertia of the ocean is slightly higher in this simulation.

The large-scale characteristics of wind stress and precipitation (Figs. 4, 5) are consistent with the temperature field. In January, the trade winds are well reproduced in the Pacific ocean in KE except in the eastern part where they penetrate too far south (Fig. 4b, left). This structure is consistent with the lack of precipitation north of the equator in this region and with the presence of a double ITCZ structure around 4°S (Fig. 5b, d, left). Along the coast of South America and South Africa the northward component of the windstress is not strong enough (Fig. 4b, left). The coastal upwelling is thus slightly damped and the surface SST warmer than observed (Fig. 1a). The windstress structure is also too zonal between 4°S and the equator in the western Pacific in January (Fig. 4b, left), as is the zonal distribution of the southern Pacific convergence zone (SPCZ, Fig. 5b, left). In July, the observed windstress is more intense in the southern hemisphere and up to 8°N in the eastern Pacific and Atlantic Ocean (Fig. 4a, right). This pattern is associated with the strengthening of the northern hemisphere Hadley cell, and with the intensification of the monsoon flow from the ocean towards the continent, where heavy precipitation occurs (Fig. 5a, right). This return flow from the ocean to the continents over America and Africa is reproduced in KE. However, windstress is not strong enough along the eastern border in July (Fig. 4b, right) where warm water accumulate (Fig. 1a). Figure 5d also shows that monsoon rainfall is underestimated over the southern border of North America, Africa and India.

These drawbacks are more pronounced in TI. In January the trade winds are too strong in the northern hemisphere and converge too far south (Fig. 4c, left), resulting in the systematic southward shift of the ITCZ compared to KE

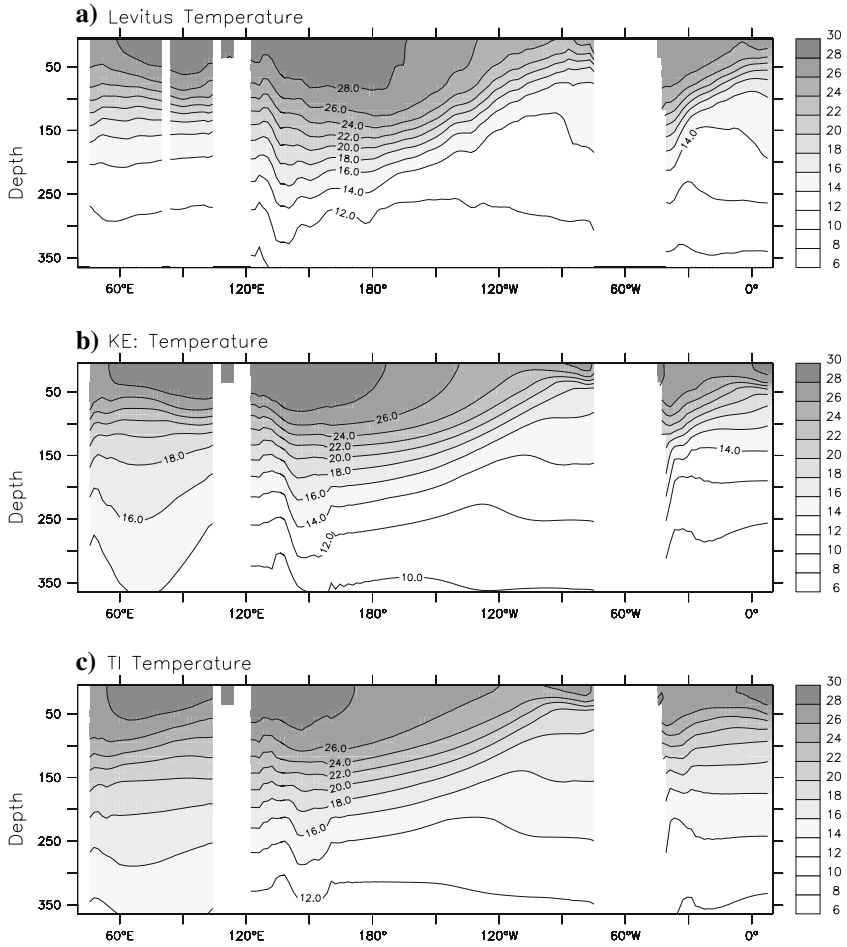

Fig. 3 Equatorial section of the upper 350 m of the ocean averaged between 2°N and 2°S for **a** Levitus (1982) climatology, **b** KE and **c** TI. Isolines are plotted every 2°C

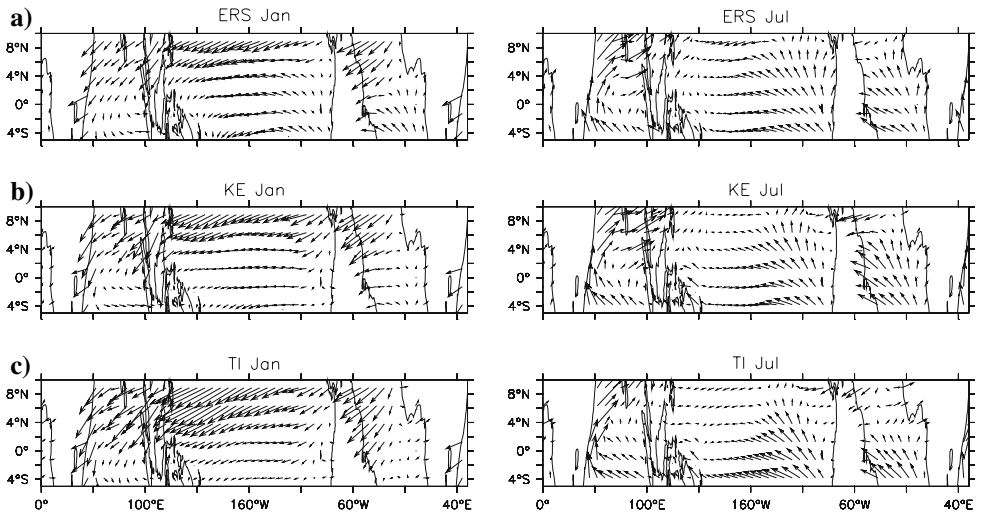

Fig. 4 January (*left*) and July (*right*) wind stress (in Pa) between –5°S and 10°S for **a** ERS data, **b** KE, and **c** TI

(Fig. 5e, left) and in the too strong precipitation over the maritime continent (Fig. 5c left). Along the equator, the maximum wind stress is also slightly shifted from the middle of the basin to the west, and there is almost no extension of the eastward (or the westerly) winds in the western Pacific (Fig. 4c, left). The Walker cell across the Indian Ocean is weaker in this simulation, which explains the reversal of the temperature gradient in the ocean interior (Fig. 3). A similar weakening was obtained in atmosphere-alone simulations (Hourdin et al. 2006). In July the

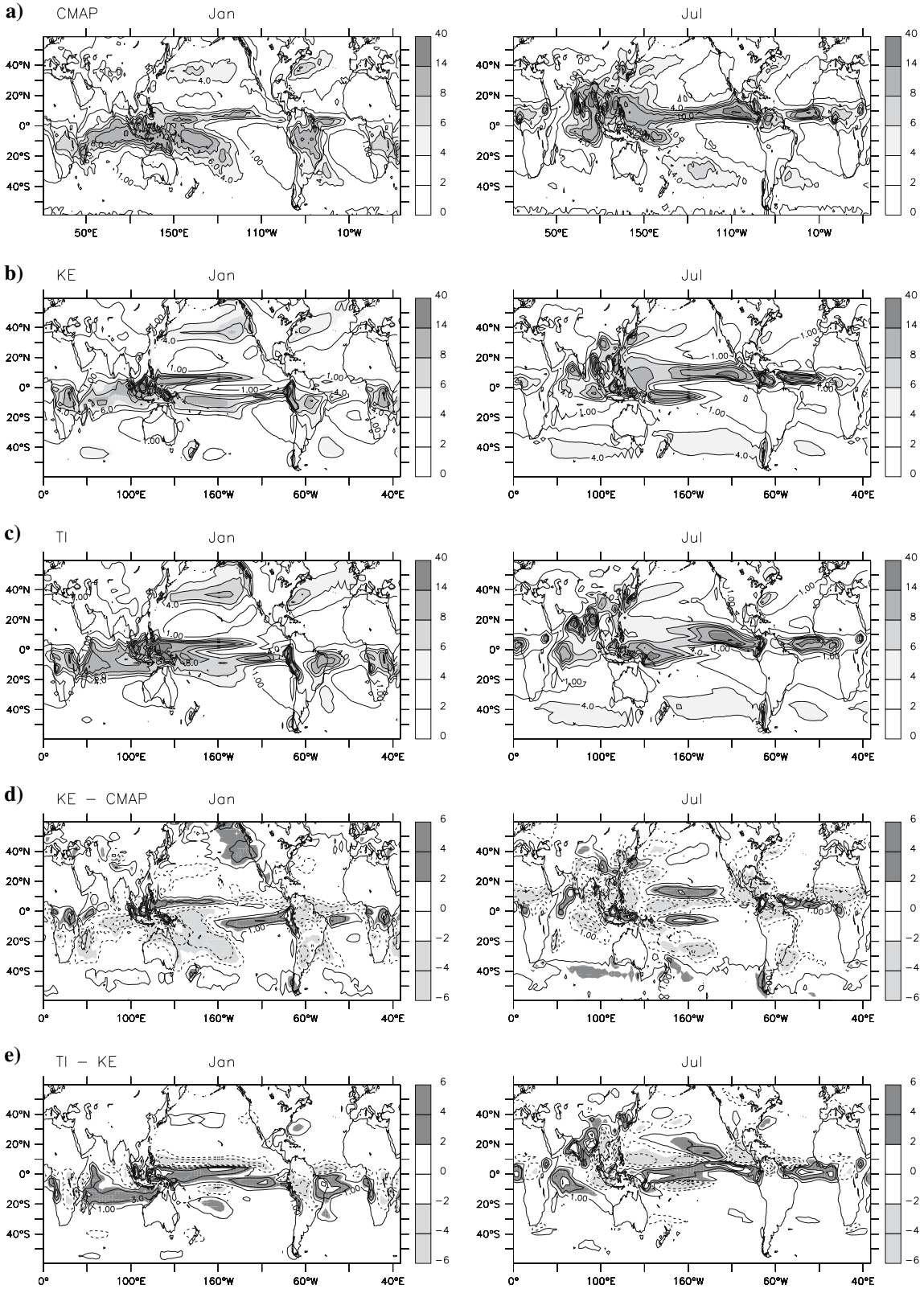

Fig. 5 January (*left*) and July (*right*) precipitation (mm day^{-1}) for a) the CMAP climatology (Xie and Arkin 1996), **b** KE, **c** TI, **d** differences between KE and climatology and **e** differences between TI and KE. In all graphs isolines are plotted every 2 mm day^{-1} (the zero line is omitted)

return flow from the ocean to the continent associated with the American and African monsoon is weak (Fig. 4c, right). In the Atlantic the Southeasterlies do not penetrate far enough during summer in the northern hemisphere, and the wind stress does not allow for the development of the ocean upwelling at the coast. It is also interesting to note that the ITCZ is shifted to the south in TI compared to KE year round in the Pacific ocean (Fig. 5e).

The above discussion shows that representation of convective clouds in the model affects the simulation of the tropical mean climate. We analyze below how this affects the seasonal cycle of tropical SST and precipitation.

3.2 Mean seasonal cycle

Figure 6 shows the mean seasonal evolution of SST and precipitation for several regions in the tropics. In KE, the phasing of the annual cycle of SST and precipitation is satisfactorily represented in most regions. However, as discussed above (comments of Fig. 1, 5), precipitation is underestimated in the West Pacific north of the equator from April to October (Fig. 6.3). In the eastern part of the basin, precipitation is overestimated from January to June (Fig. 6.4). This excess of precipitation is associated with an excessive surface warming during the same period. This feature corresponds to the double ITCZ structure that develops over a longer period and with a larger magnitude than in the observations. A similar feature is present in the Atlantic ocean, where the SST is too warm from November to June and where the precipitation is overestimated from January to June south of the equator (Fig. 6.6). The phasing of the annual mean cycle of SST and precipitation is less satisfactory in TI. In particular the development of the double ITCZ and the associated warm surface conditions lasts longer in this simulation and the magnitude is larger. In the Indian ocean, the semi-annual cycle of SST is misrepresentated (Fig. 6.1 and 6.2). The convection scheme has thus a major impact on the representation of ocean surface and subsurface temperature characteristics in this region.

Figure 7 displays the geographic distribution of the seasonal cycle of the simulated and observed SST in the tropics. For simplicity, we characterize the seasonal cycle and assess it against observations by considering its magnitude (quantified here as the difference between the monthly maximum and the monthly minimum temperatures estimated from a mean seasonal cycle) and the correlation between the simulated and observed seasonal cycle of SST. Results for the magnitude are plotted for each grid point as the ratio of the difference between model and observation to observation. Figure 7a, b and c show that the two model versions tend to underestimate the magnitude of the seasonal cycle in the eastern part of the Pacific and Atlantic oceans, where SSTs are warmer than observed on average (Fig. 1). In TI, this underestimate reaches 50% over large regions, whereas it is around 20% in KE. In the western Atlantic, we note an excessive magnitude of the seasonal cycle in KE (Fig. 7b), which is associated with the westward shift of the equatorial upwelling. The correlation between the observed and simulated seasonal cycles of the SST characterizes the ability of the model to reproduce the phasing of the seasonal SST anomalies. Figure 7d and e show that it is better in KE in most places.

The evolution of the seasonal cycle along the equator averaged between 2°N and 2°S (Fig. 8) shows that both simulations produce a timing of the equatorial upwelling in phase with the observations. However the westward shift of the upwelling core and the westward propagation in the Pacific are more pronounced in TI (Fig. 8). From experiments with an intermediate coupled model, Fu and Wang (2001) suggested that the westward propagation of the cold tongue was mainly due to the zonal advection of cold water by the oceanic circulation. This is the case in TI where the zonal current is more intense west of 140°W due to the stronger trade winds in these regions (Fig. 4). In the Atlantic, the magnitude and the phase of the equatorial upwelling are satisfactory in KE although its core is shifted to the west. As already noted, this seasonal modulation of the equatorial upwelling nearly vanishes in TI.

4 Tropical oceans and seasonal march of the ITCZ

4.1 In the eastern Pacific

The analysis of the mean seasonal cycle shows that the convection and cloud schemes strongly impact the representation of both the mean state and the seasonal characteristics of the climate in the eastern part of the Pacific ocean. We now analyse this in more depth, considering first the region extending from 110°W–90°W to 8°S–14°N (left shaded box in Fig. 6). This region allows us to analyse the development of the equatorial upwelling and the connection between the equatorial SST and the location of the ITCZ. In this region SST exhibits a well defined seasonal cycle, with warm waters located south of the equator in boreal spring and shifting to the north of the equator from June to September as the equatorial and coastal upwelling intensifies from 8°S to 2°N (Fig. 9 left).

Several aspects of the wind and cloud fields have been identified as important players in this feature. The upwelling along the coast of Peru and the equatorial upwelling in the east fully develop when the wind blows along the coast of South America and intensifies to the north. At that time, the zonal component of the windstress

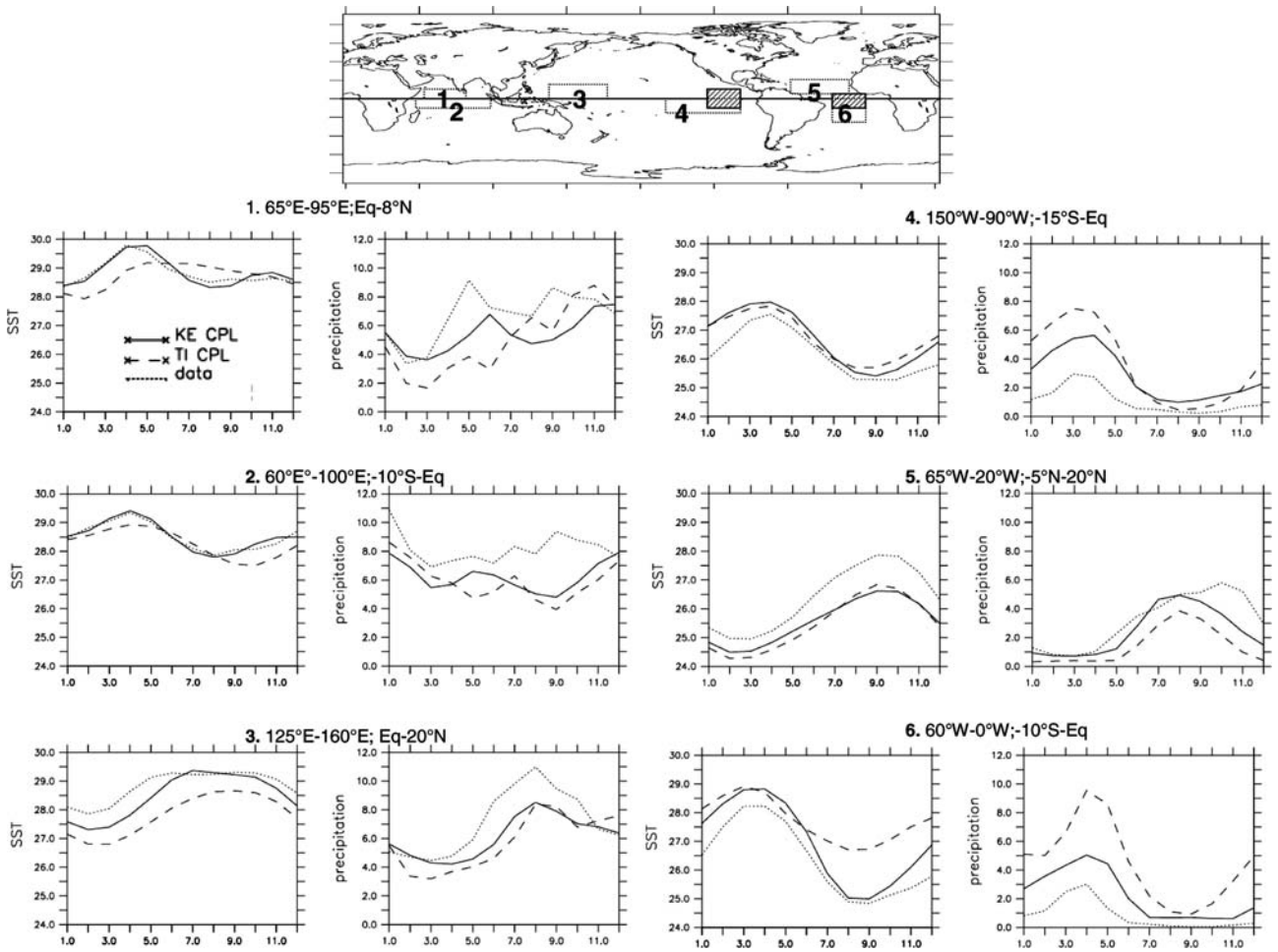

Fig. 6 Comparison of mean seasonal cycle of SST (°C) and precipitation (mm day^{-1}) for KE (*solid line*), TI (*dashed line*) and observations (*dotted line*), for several boxes over the tropical ocean. The box limits are identified by the rectangles on the map, and referenced by a number (1–6). The two hatched boxes correspond to the regions used to in Sect. 4

also intensifies along the equator towards the west, which enhances the equatorial divergence and allows for the strengthening of the equatorial upwelling further west. The onset of American summer monsoon on the continent at 15°N seems to be an important factor in this intensification and in the position of the core of the equatorial upwelling near the coast (Wang 1994). Several feedbacks, involving SST, clouds or wind and evaporation enter then into play to reinforce the upwelling and maintain the ITCZ in a northern position (e.g. Xie and Saito 2001).

As mentioned above (Figs. 8, 9b left), the seasonal evolution of the equatorial upwelling is quite realistic in KE. In particular, the northward SST gradient between the cold tongue and the warmer water to the north is present in KE from July to November (Fig. 9b left). This is consistent with the onset and the maintenance of the cross equatorial monsoon flow in this simulation (Fig. 4b right). Note however that the structure is slightly shifted towards the equator, and that warm waters are not warm enough north of 8°N, as suspected from the wind stress and the lack of precipitation over the continent (Fig. 5d right). As the SST gradient intensifies to the north (April–May), precipitation follows quite closely the region of maximum surface temperature in the northern hemisphere (Fig. 9b left). In boreal winter and early spring, the maximum precipitation is located as in the observations above warm waters around 4°S, peaking in March.

Figure 10b also shows that the total cloud cover intensifies within the ITCZ as well as south of the equator over the cold waters from July to October. In the latter regions, air is subsiding and clouds are limited to lower tropospheric levels. They reduce the incoming solar radiation at the ocean surface and cool the surface. Therefore this version of the model produces an annual variation of low level clouds consistent with a local strengthening of the meridional circulation in the eastern Pacific as shown by Ma et al. (1996).

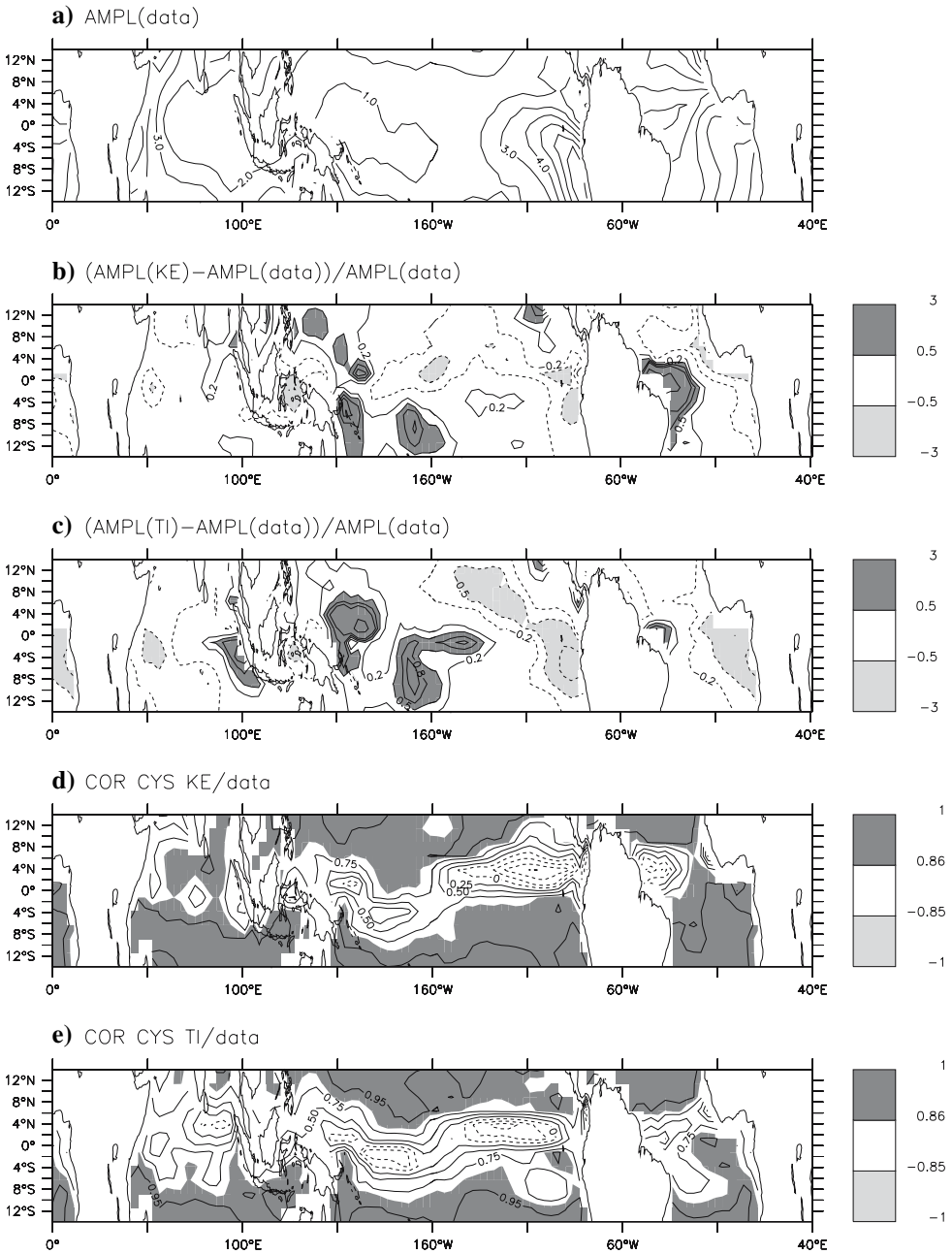

Fig. 7 Comparison of the characteristics of the simulated mean seasonal cycle of SST with the Reynold's (1988). **a** Annual mean cycle as estimated from data, **b** and **c** ratio of the difference between the simulated and observed annual mean SST amplitude (defined as the maximum minus the minimum of the monthly temperature) to the observed amplitude for TI and KE respectively. **d** and **e** Correlation between the simulated seasonal cycle at each model grid point with the observation for TI and KE. The data have been interpolated on the model grid. *Solid lines* stand for positive values, *dashed lines* for negative values

The TI simulation exhibits a different behaviour in this region. Interestingly, the seasonal cycle is pretty well simulated until April–May (Fig. 9c, left), but the whole structure retreats back to a more equatorward position in July and the SST gradient becomes weak (Fig. 9c left). Then the ITCZ develops over a kind of SST plateau. The reduced SST gradient reduces the wind stress along the equator and the equatorial divergence, which damps the development of the equatorial upwelling. Also large differences are found between the two simulations in the representation of the cloud cover (Fig. 10). In TI (Fig. 10c left) the maximum cloud cover follows the ITCZ. It is thus maximum where deep convection occurs, and the cloudiness is weak in subsidence regions. Figure 10d also shows that during the peak development of the equatorial upwelling (July–November) these differences in cloud cover between the two simulations lead to a difference of about 80 W/m^2 in the cross equatorial contrast in net surface shortwave flux, between 4°S and 4°N. Therefore in TI the seasonal evolution of the cloud cover damps the SST gradient across the equator, and thereby reduces the strength of the wind along the equator and the strength of the equatorial upwelling.

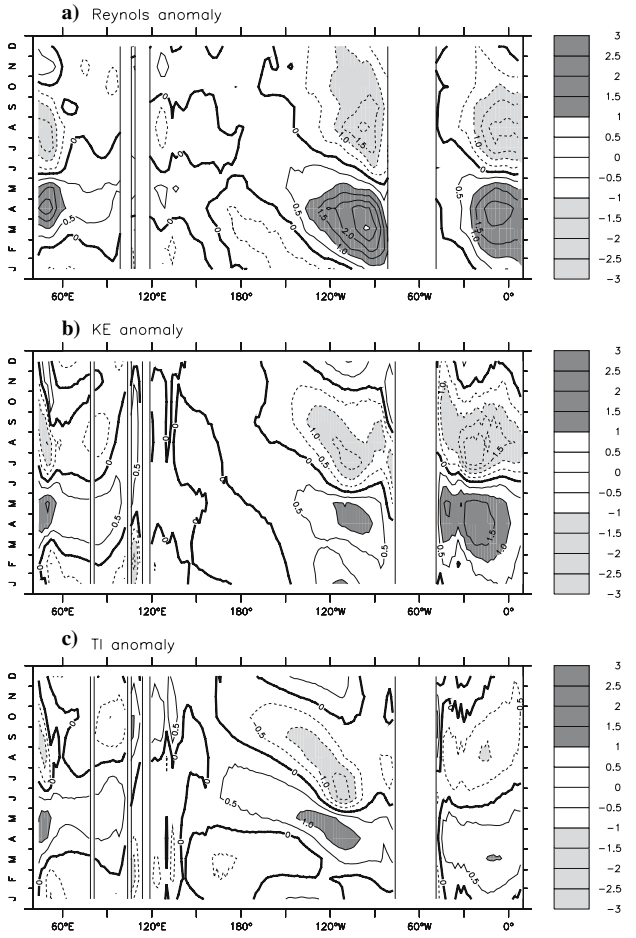

Fig. 8 Seasonal mean evolution (annual mean removed) of SST (°C) along the equator averaged between 2°N–2°S for **a** Reynolds' (1988) climatology, **b** KE and **c** TI

Figure 11 summarizes the differences between the two simulations averaged for the region 90° W to 110° W during the peak development of the upwelling (August–November). Even though KE exhibits systematic differences with observations, it exhibits sharp SST and 2 m air temperature gradient across 2°N (Fig. 11a, b). Precipitation over the ocean properly follows the observations (Fig. 11c). Low level specific humidity increases northwards, with maximum values around 8°N and minimum values in the southern hemisphere (Fig. 11d). Several characteristics found in KE are in good agreement with the data reported by Pyatt et al. (2005) along 95°W. Specific humidity is however slightly overestimated (by about 2 g/kg) compared to observation (Fig. 11d). On the other hand neither the flat SST distribution across the equator nor the uniform distribution of humidity found in TI are realistic. In this simulation, the convergence of humidity, the maximum precipitation, and surface cooling by clouds occur at the same location (about 4°N).

4.2 In the Atlantic

The variability of the equatorial Atlantic shares some similarities with the eastern Pacific both at the annual and interannual time scales (Chiang and Vimont 2004). Since in KE the equatorial upwelling develops in the middle of the basin rather than along the coast (Fig. 8), we adjusted a box so as to capture its seasonal evolution. Figures 9 right and 10 right consider thus the zonal average of surface conditions between 30°W and 7°E. The northern limit is provided by the position of the continent in the northern part of the Gulf of Guinea (5°N), so that we limit the latitudinal extension from 8°S to 4°N. Therefore the intensity of the equatorial upwelling is slightly reduced in the observation since the core of the upwelling is located further east. However, the seasonal evolution of SST and precipitation is well depicted in these figures. From January to June, warm waters and precipitation associated with deep convection within the ITCZ expand down to 8°S. From July to November, cold waters develop from 8°S to 1°N and warm waters and precipitation are located further north (Figure 9a right).

For this basin, differences in the representation of the equatorial upwelling and in the location of the ITCZ between TI and KE are quite similar to those found in the eastern Pacific (Figs. 9, 10). They are even larger. In KE, the seasonal march of the ITCZ over this region follows quite closely that of the SST (Fig. 9b right). The timing of the north–south migration of the ITCZ across the equator is well represented. It corresponds to the intensification of the trade winds across the equator and to the eastward convergence of winds over the African continent (Fig. 4, right) where monsoon precipitation occurs (Fig. 5b). The monsoon flow and the precipitation do not develop as far north as in the observation, which explains why the zero line of the SST field in Fig. 9b (right) does not cross 2°N. During the peak of the upwelling, when warm waters and the ITCZ are in their northern position, cloud cover is substantial both in the ITCZ and over the cold waters just south of the equator (Fig. 10b right). In the latter regions these clouds reduce the incoming solar radiation at the surface and contribute to cool the surface, like in the Pacific ocean. In TI (Fig. 9c right), the upwelling does not develop and convection is maximum over a very weak SST gradient, like in the Pacific ocean. The overall feature is consistent with the windstress field (Fig. 4). In TI, the windstress is not strong enough across and along the equator, and so is the return flow towards Africa. The convection is more active over the ocean in TI than in KE, as shown by the 500 hPa large-scale vertical velocity in Fig. 10 (right). The cloud cover develops within the ITCZ in TI. Like in the Pacific, the net effect of these clouds is to damp the meridional SST gradient in this simulation (Fig. 10).

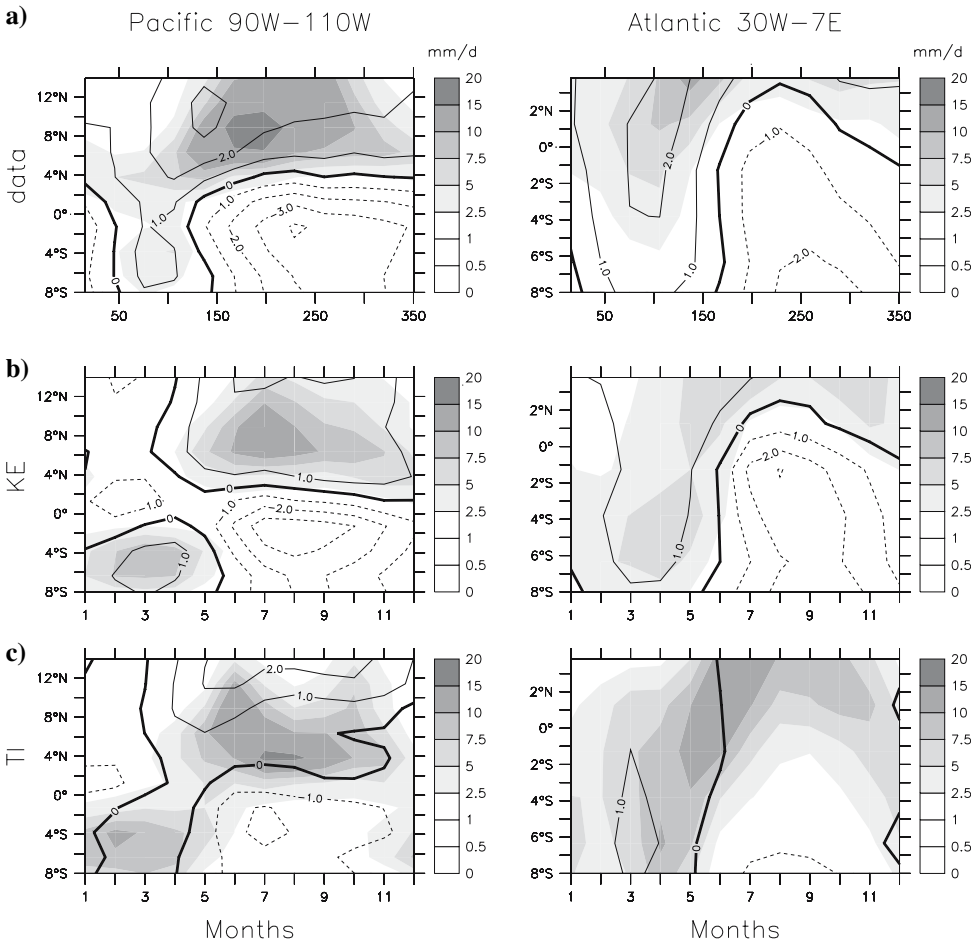

Fig. 9 Mean seasonal cycle of SST (annual mean of the box removed; isolines; °C) and precipitation (*shading*; mm day^{-1}) averaged from 90°W to 110°W in the Pacific (*left*) and from 30°W to 7°E in the Atlantic (*right*) and plotted as a function of latitude and time for **a** the Reynold's SST and CMAP precipitation climatologies, **b** KE and **c** TI

Convection and precipitation in KE are strongly linked to SST. We compute for each month the spatial correlation between SST and rainfall over the tropical (30°S–30°N) Atlantic and Pacific for the two simulations (Fig. 12). We also compute this correlation from CMAP (Xie and Arkin 1996) climatology of precipitation and Reynolds' (1988) climatology of SST. Figure 12 shows that the seasonal evolution of this correlation is quite satisfactorily represented in KE. The correlation is however a little bit too strong with KE, wich may be related to the fact that the parameterization is very sensitive to the low level static energy, strongly controlled by the SST (a common bias in AGCM, Biasutti et al. 2006), and probably not sensitive enough to other parameters such as the upper boundary layer and free troposphere humidity (Derbyshire et al. 2004; Grandpeix et al. 2004). On the other hand, the correlation is poor for TI (Fig. 12), and even not significant during boreal summer, certainly because SST has no well defined structure in the equatorial regions in this simulation. During boreal winter the convergence occurs where SST is maximum south of the equator near South America, which explains the better correlation found for this period.

5 Interaction between convection, clouds and the large-scale circulation

Our analyses show that KE and TI exhibit similar differences in the eastern Pacific and equatorial Atlantic basins. The seasonal cycle of the equatorial upwelling is better reproduced in the simulation where the cross equatorial wind stress is stronger, and in which the wind convergence toward the continent is sustained. This is in agreement with Xie and Saito (2001), who show that the presence of a bulge of landmass was important to determine the meridional structure of the ocean ITCZ in the east, and with Fu and Wang (2001), who identified the meridional wind stress as a critical parameter in the development of the equatorial upwelling in the east Pacific.

The differences between the two simulations presented here involve the connection between cross-equatorial trade wind, the monsoonal return flow over southern North America or West Africa, and the cloud cover. The way the convection and cloud schemes interact with the large-scale circulation is further discussed from atmosphere-alone re-

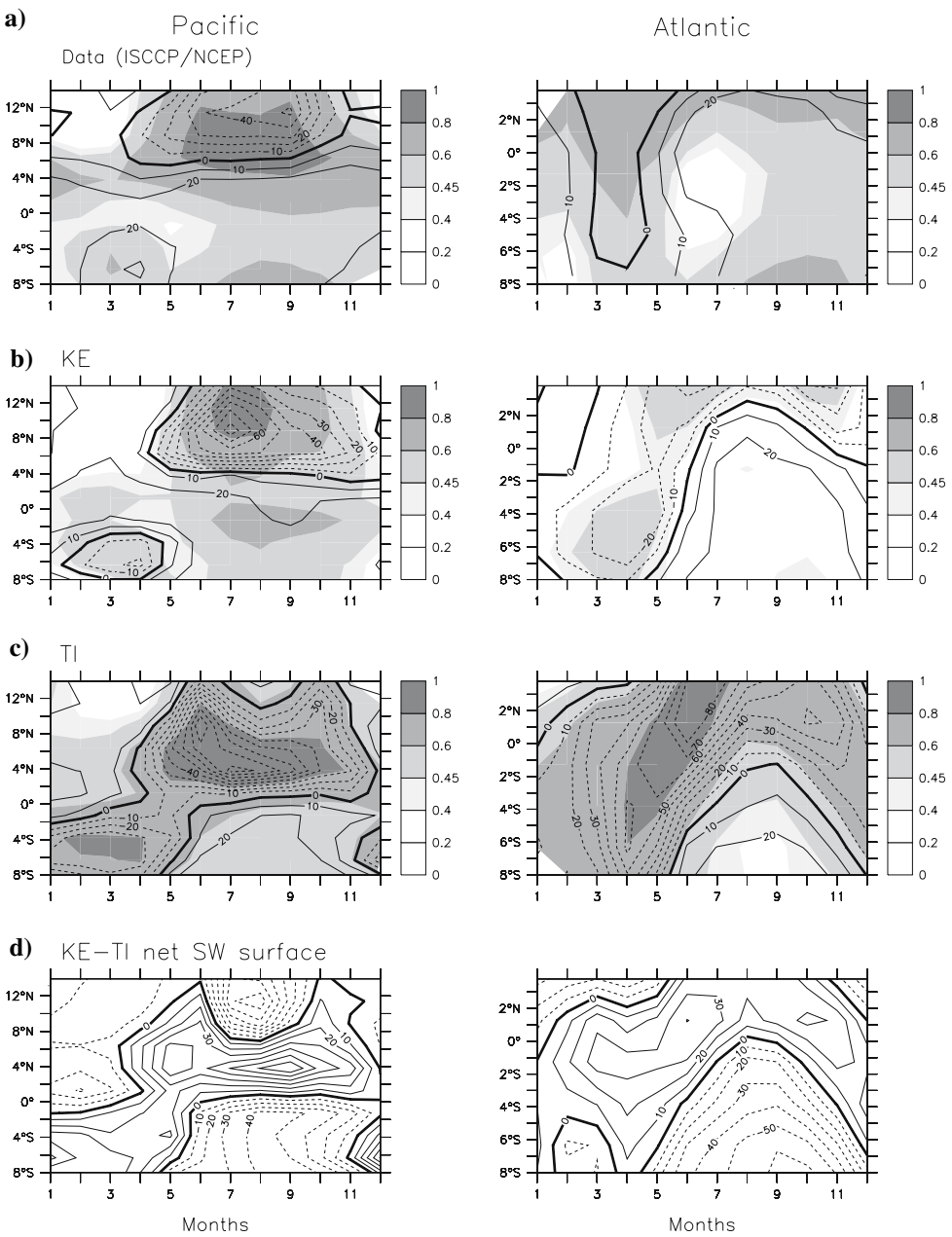

Fig. 10 Same as Fig. 9 for **a** to **c**, but for the mean seasonal cycle of ω500 hPa (hPa day^{-1}, isolines) and total cloud fraction (*shading*). **d** Difference (TI – KE) of surface net shortwave flux simulated at the surface in the same regions. In **d**, the annual mean value over the region was subtracted from each simulation before computing the difference to better emphasize the gradients and the seasonal cycle

sults (Hourdin et al. 2006). Then we discuss the ocean feedback.

5.1 Link with the characteristics of convection and cloud radiative forcing

We first compare the behaviour of tropical clouds and convection simulated in the atmospheric and coupled versions of the model. We use the analysis sorted by dynamical regimes of Bony et al. (2004), and consider the monthly mean 500 hPa vertical velocity (ω500) as a proxy for large-scale vertical motions in the atmosphere. For the different circulation regimes, we compare the mean cloud radiative forcing (CRF) derived from coupled and uncoupled experiments for each version of the convective cloud schemes (Fig. 13). Note that the probability distribution function (PDF) of ω500 remains the same for coupled and uncoupled experiments (not shown).

For the different regimes, the CRF of the coupled simulations are similar to those found in the atmosphere alone simulations. In KE the CRF is overestimated (up to 12 Wm^{-2} for the latter) in regimes of moderate convection (–40 hPa/day < ω500 < –20 hPa/day). The net CRF at the top of the atmosphere from TI is more negative (by about 10 Wm^{-2}) than that from KE and satellite data in all convective regimes (ω500 < 0 hPa/day). Figure 13c shows

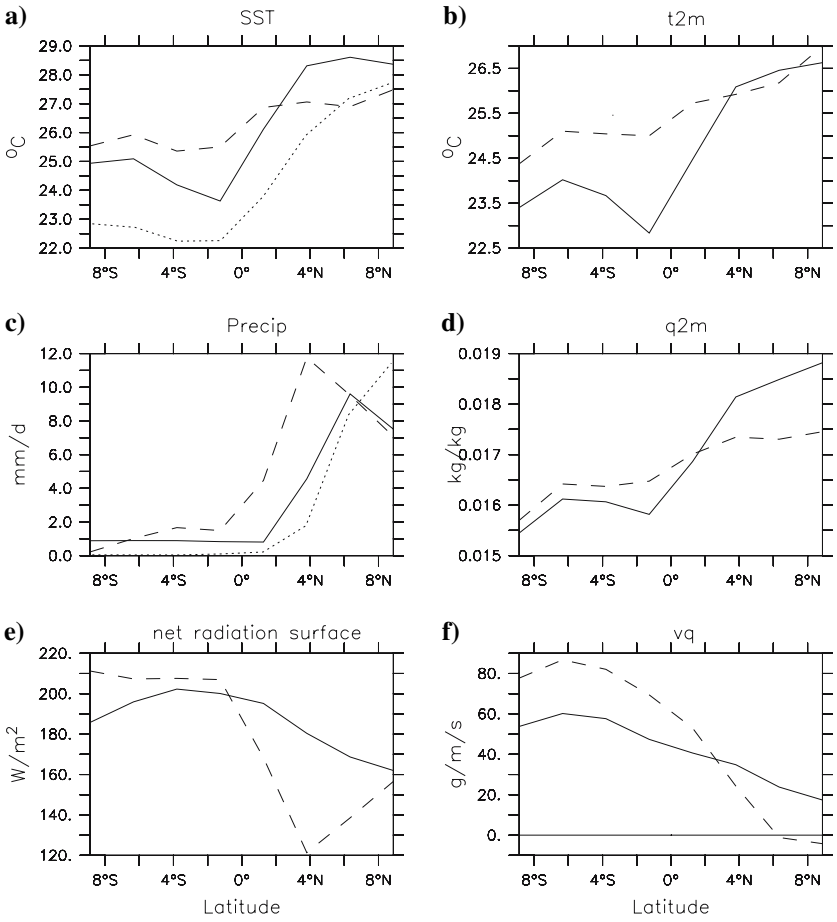

Fig. 11 Cross equatorial section averaged from 90°W to 110°W and from August to November of **a** SST (°C), **b** 2 m air temperature (t2m, °C), **c** precipitation (Precip, mm day^{-1}), **d** 2 m air specific humidity (q2m, kg/kg), **e** net shortwave radiation at the surface (Wm^{-2}, positive downward), and **f** the meridional latent heat transport integrated over the atmospheric column (vq, g m^{-1} s^{-1}). In each graph, the *solid line* represents KE and the *dashed line* TI. In **a** and **c** the *dotted line* stands for the observations (CMAP for precipitation and Reynolds for SST)

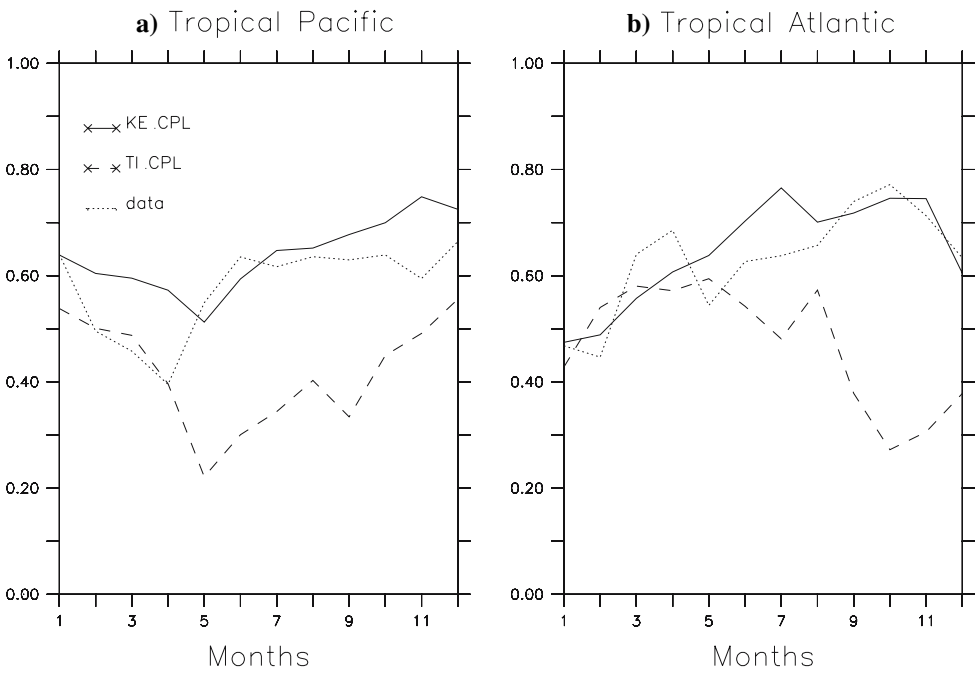

Fig. 12 Spatial correlation between precipitation and SST computed for each month between 30°N and 30°S for z**a** the Pacific ocean and **b** the Atlantic ocean. In each graph, the *solid line* represents the estimation from KE, the *dashed line* the results from TI and the *dotted line* an estimate from the Reynold's (1988) and CMAP climatologies

that this difference at the top of the atmosphere partly translates to the surface (the SW CRF at the surface is more negative in TI than in KE). So, in TI, the cloud cover of the ITCZ leads to a stronger cooling at the surface and to a reduced SST gradient with surrounding areas than in KE. This is consistent with the colder conditions found in the

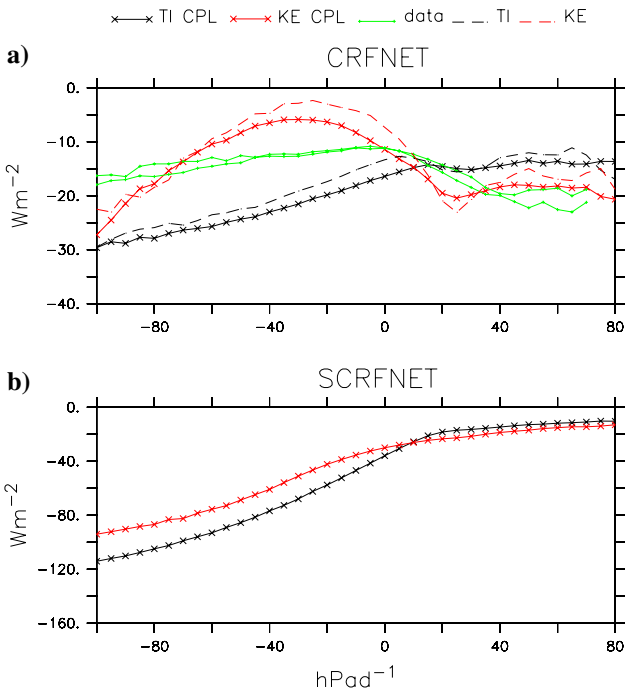

Fig. 13 Regime sorted plots as a function of ω500 in hPa day^{-1} between 30°N and 30°S over the ocean for a) the net cloud radiative forcing a the top of the atmosphere (Wm^{-2}), b) the net cloud radiative forcing at the ocean surface (Wm^{-2}). In all graphs the black lines stand for simulations with the Tiedtke convection scheme and the *red lines* for simulations with the Emanuel convection scheme. In **a** and **b** the coupled simulations are represented by the *solid lines* and AMIP type simulations with the atmospheric model by the dashed lines. For comparison two estimates from ERA40 and NCEP reanalyses for ω500 and ERBE (Barkstrom 1984) for cloud radiative forcing are included

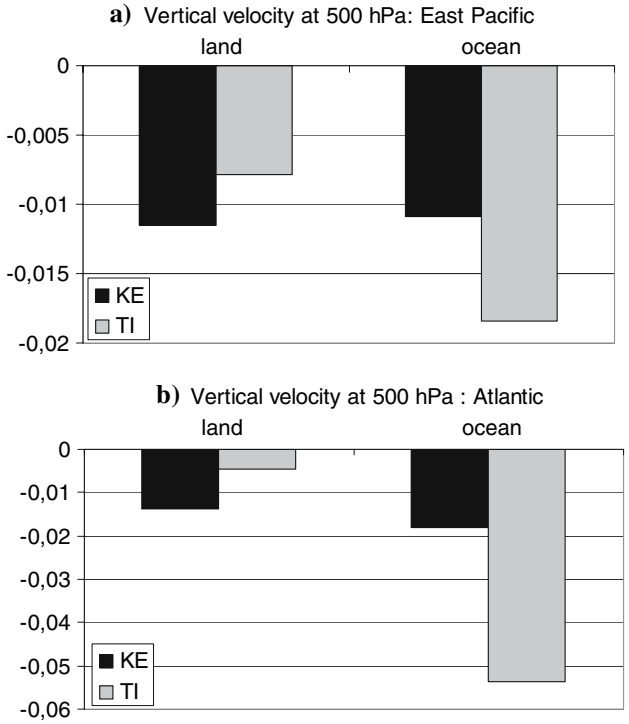

Fig. 14 Bar charts representing the 500 hPa (hPa s^{-1}) vertical velocity averaged over land and ocean from June to October in TI and KE for the Eastern Pacific (100°W–80°W; 0°N–20°N) and Atlantic (20°W–7°E; 0°N–20°N)

west Pacific in TI (Fig. 1). In subsidence regimes (ω500 > 0 hPa/day, which generally occurs over cold waters), the cooling effect of clouds is underestimated in TI, which also contributes to reduce the SST contrasts with surrounding regions.

The regime sorted analysis also shows a very similar behaviour of the warming and moistening of the atmospheric column by convection in the coupled and atmosphere-alone simulations, both over the ocean and over land (not shown). Analyses of the atmosphere-alone simulations by Hourdin et al. (2006) suggest that the better representation of land–sea contrasts in rainfall and cloud radiative forcing with the Emanuel's scheme comes from the representation of downdraughts over the ocean. In KE, convection is inhibited by downdraughts both over land and over ocean. In TI, the convection over ocean is not damped by convective downdraughts as it is the case in KE, which leads to more vigorous ascents (Fig. 10c). As a result, convection in TI is better sustained over ocean than over land while in KE it is comparable over ocean and land. This systematic difference between the two simulations is particularly clear for June to October (Fig. 14) for the eastern Pacific and Atlantic. Convection is more active in TI over ocean, whereas similar ascending motions are found in KE over ocean and land. The situation is even more contrasted for TI in the Atlantic (Fig. 14b). This effect is more pronounced in coupled than in atmosphere alone simulations because of the feedback with SST, as explained below.

5.2 Monsoon flow, clouds and SST in the eastern part of the Pacific and Atlantic

In KE, several feedbacks from the atmospheric circulation come into play in the coupled model to cool down the SST along the equator and to enhance the SST gradient in the East Pacific and Atlantic. In TI the feedbacks act to damp the SST gradients and the ITCZ remains rather south. These feedbacks involve both the ocean circulation and the cloud cover.

Figure 15a shows that in August–September, during the peak development of the upwelling, the zonal currents in the upper layer of the ocean model (upper 10 m) are smaller in KE than in TI in the eastern Pacific. The reversal of the westward south equatorial current and the eastward north equatorial current is located at 4°N against 3°N in TI.

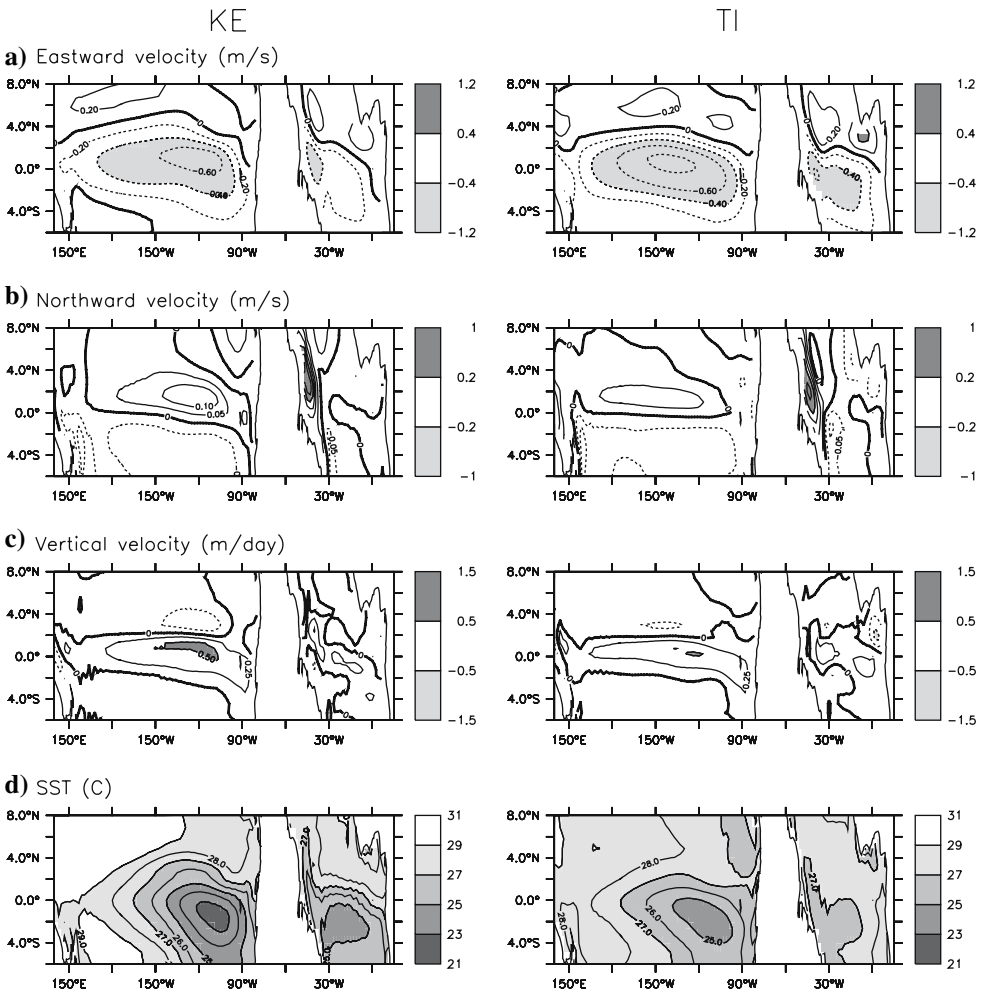

Fig. 15 Ocean currents for the upper layer of the ocean model and SST in August in the Pacific and Atlantic for TI (*left*) and KE (*right*). **a** Zonal current (m s^{-1}), **b** meridional current (m s^{-1}), **c** vertical velocity at the base of the upper layer (m day^{-1}), and **d** SST (°C)

On the contrary, the meridional component of the current, and the vertical velocity at the base of the upper layer are stronger in KE across the equator (Fig. 15b, d). Upwelled waters cool the surface, and the meridional component of the current advects northwards cold water from the south of the equator. The meridional windstress component across the equator and its convergence to the north of it are thus two critical features that help maintain cold water along the equator and a sharp SST gradient to the north of it. This SST gradient locally enhances the windstress. The role of vertical and meridional temperature advection in cooling the surface layer is less active in TI (Fig. 15b, c). Also since the thermocline is more diffuse in TI (Fig. 3), upwelled waters are warmer, reducing the cooling effect of the upwelling. Note that in the Atlantic ocean, the components of the currents are more similar between the two simulations. The major differences come from warmer upwelled waters in the upper layer.

As seen in Sect. 4, the cloud cover further contributes to enhance the SST gradient in KE and to damp it in TI (Fig. 10). In KE, the SST gradient between the cold equatorial waters and the regions further north is reinforced by the presence of low level clouds over cold waters (Fig. 10d). The stronger SST gradient maintains the wind stress and the development of the equatorial upwelling. In TI, the development of the equatorial upwelling is not sufficient to maintain a sharp cross equatorial SST gradient that would reinforce the windstress. In addition convective clouds strongly cool down the surface where convection occurs (Figs. 10, 13), which further contributes to weaken the SST gradient, and to reinforce the southward shift of the ITCZ.

6 Conclusion

The comparison of two coupled ocean–atmosphere simulations performed with different convective cloud schemes allows us to investigate how the representation of clouds and convection interacts with the large-scale tropical atmospheric and oceanic circulations. The simulated mean state and the seasonal cycle of the SST in most part of the

equatorial ocean differ strongly depending on the convection and clouds scheme used. As suggested by previous studies, the cross equatorial wind in the eastern Pacific and in the Atlantic during boreal summer is critical to maintain the equatorial upwelling, and the advection of cold waters to the north of the equator. The simulation that best represents the position of the ITCZ in these regions is the simulation for which the cross equatorial circulation is more active, and in which convection is well sustained over the continent. The fact that convection is sustained or not over land is attributed to the inhibition of convection by downdrafts, which stresses the important role of this part of the parameterization on the large scale pattern of the tropical climate.

To first order, the major characteristics of the surface climate simulated by the coupled model resemble those of atmosphere alone simulations. Indeed the distribution of cloud radiative forcing and convection regimes in the tropical regions is the same in the coupled simulations as in simulations with the atmospheric model forced by prescribed SST. In addition the land–sea contrast in precipitation shares lots of similarities with the atmospheric simulations. The study also confirms the relevance of the regime-sorted analysis, which allows to characterize the behaviour of the parameterization in a synthetic way.

The key role of atmospheric processes on coupled simulations has been noted in other studies considering several ocean models coupled to the same atmospheric model. For instance, Guilyardi et al. (2004) found that the atmosphere had a dominant role in setting El Niño characteristics (periodicity and base amplitude) and errors (regularity) in coupled models. When analyzing the climate sensitivity of different NCAR models, using different combinations of oceanic and atmospheric models, Meehl et al. (2004) concluded that the atmospheric model ''manages'' the relevant global feedbacks including sea ice albedo, water vapor, and clouds.

In the simulations presented here, we show that feedbacks from the ocean circulation amplify the differences found in atmosphere-alone simulations. In particular, differences in the atmospheric simulations propagate down to about 1,000 m in the ocean interior. Our analysis also shows that the interaction between convection, clouds and the large-scale tropical circulation plays a key role in the simulation of the seasonal variations of the SST. In the simulation where convection is inhibited by downdrafts both over the continent and the ocean (KE), the monsoon flow converging in south North America and Africa is better reproduced, and this reinforces the maintenance of the inland moisture convergence. In the simulation (TI) where convection is not inhibited by downdrafts over the ocean, convection and moisture convergence are too strong over the ocean, and favor the large-scale convergence over the ocean at the expense of that over the continent. The ITCZ is thus located further south all year round in this simulation. This mechanism is reinforced by the radiative impact of the cloud cover. In one case (TI) the cloud cover tends to cool the surface in (warm) regions of convection whereas in the other case (KE), the cloud cover is more uniform between convective and subsiding regions, which reinforces the SST contrasts between (cold) subsidence regions and (warm) convective regions, and hence the windstress and the equatorial upwelling. In both cases the feedback from the ocean circulation leads to SST patterns that enhance these basic mechanisms.

These results clearly show that understanding the coupled system requires to consider in an integrated way the evolution of the seasonal cycle over land and over ocean, since they are interconnected through the atmospheric large-scale circulation. The investigation of the relative strength of deep convection between ocean and land in several models is thus likely to help us to understand why different climate models produce different mean climate states and seasonal cycles in the tropics. Our analysis also suggests that a model assessment should be based not only on the evaluation of the model's climatology by comparing observed and simulated fields, but also on the evaluation of key mechanisms. The comparison with climatology reveals that both simulations have serious biases compared to observations. However, when going into the details, it becomes clear that the KE simulation better represents several major features of the mean climate and of the seasonal cycle in the tropical regions. The differences in the parameterization between these two simulations also have an impact on the interannual variability simulated by the coupled model. This will deserve future investigation, and will be considered in a forthcoming study.

Acknowledgments We would like to thank all IPSL people who participate to the development of the IPSL_CM4 model. We also thank Laurent Fairhead for the introduction of the convection schemes in the LMDZ model, and Ionela Musat for the adjustments of the climatology. Computer time was provided by Centre National de la Recherche Scientifique (IDRIS computing center) and Commissariat à l'Energie Atomique (centre CCRT computing center). This work is a contribution to the european project ENSEMBLES (Project no. GOCE-CT-2003-505539) and to the french project PNEDC-MC2.

References

Barkstrom BR (1984) The earth radiation budget experiment (ERBE). Bull Am Meteorol Soc 65:1170–1185

Bentamy A, Quilfen Y, Gohin F, Grima N, Lenaour M, Servain J (1996) Determination and validation of average wind fields from ERS-1 scatterometer measurements. Global Atmos Ocean Syst 4(1):1–29

Biasutti M, Sobel A, Kushnir Y (2006) Agcm precipitation biases in the tropical atlantic. J Clim 19(6):935–958

Bony S, Dufresne JL, Le Treut H, Morcrette J, Senior C (2004) On dynamic and thermodynamic components of cloud changes. Clim Dyn 22(2–3):71–86

Bony S, Emanuel KA (2001) A parameterization of the cloudiness associated with cumulus convection; evaluation using toga coare data. J Atmos Sci 58(21):3158–3183

Braconnot P (1998) Tests de sensibilité avec le modèle d'atmosphère du lmd, en vue d'améliorer le couplage avec l'océan. note technique IPSL 2:39

Braconnot P, Joussaume J, Marti O, de Noblet N (2000) Impact of ocean and vegetation feedback on 6 ka monsoon changes. Canada, WCRP-111, WMO/TD-No. 1007

Chiang J, Vimont D (2004) Analogous pacific and atlantic meridional modes of tropical atmosphere–ocean variability. J Clim 17(21):4143–4158

Davey MK, Huddleston M, Sperber KR, Braconnot P, Bryan F, Chen D, Colman RA, Cooper C, Cubasch U, Delecluse P, DeWitt D, Fairhead L, Flato G, Gordon C, Hogan T, Ji M, Kimoto M, Kitoh A, Knutson TR, Latif M, Le Treut H, Li T, Manabe S, Mechoso CR, Meehl GA, Power SB, Roeckner E, Terray L, Vintzileos A, Voss R, Wang B, Washington WM, Yoshikawa I, Yu JY, Yukimoto S, Zebiak SE (2002) Stoic: a study of coupled model climatology and variability in tropical ocean regions. Clim Dyn 18(5):403–420

Derbyshire SH, Beau I, Bechtold P, Grandpeix JY, Piriou JM, Redelsperger JL, Soares PMM (2004) Sensitivity of moist convection to environmental humidity. Q J R Meteorol Soc 130(604):3055–3079

Dufresne JL, Grandpeix JY (1996) Raccordement des modèles thermodynamiques de glace, d'océan et d'atmosphère. Note Interne 205, L.M.D

Dufresne JL, Quaas J, Boucher O, Denvil S, Fairhead L (2005) Contrasts in the effects on climate of anthropogenic sulfate aerosols between the 20th and the 21st century. Geophys Res Lett 32(21). doi:10.1029/2005GLO23619

Dufresne JL, Friedlingstein P, Berthelot M, Bopp L, Ciais P, Fairhead L, Le Treut H, Monfray P (2002) On the magnitude of positive feedback between future climate change and the carbon cycle. Geophys Res Lett 29(10):1405

Emanuel KA (1993) A scheme for representing cumulus convection in large-scale models. J Atmos Sci 48:2313–2335

Fichefet T, Maqueda MAM (1997) Sensitivity of a global sea ice model to the treatment of ice thermodynamics and dynamics. J Geophys Res-Oceans 102(C6):12609–12646

Fu X, Wang B (2001) A coupled modeling study of the seasonal cycle of the pacific cold tongue. Part i: Simulation and sensitivity experiments. J Clim 14(5):765–779

Gordon C, Rosati A, Gudgel R (2000) Tropical sensitivity of a coupled model to specified isccp low clouds. J Clim 13(13):2239–2260

Grandpeix JY, Phillips V, Tailleux R (2004) Improved mixing representation in Emanuel's convection scheme. Q J R Meteorol Soc 130(604):3207–3222

Guilyardi E, Gualdi S, Slingo J, Navarra A, Delecluse P, Cole J, Madec G, Roberts M, Latif M, Terray L (2004) Representing El Niño in coupled ocean–atmosphere gcms: the dominant role of the atmospheric component. J Clim 17(24):4623–4629

Hourdin F, Musat I, Bony S, Braconnot P, Codron F, Dufresne JL, Fairhead L, Filiberti MA, Friedlingstein P, Grandpeix JY, Krinner G, Levan P, Li ZX, Lott F (2006) The lmdz4 general circulation model: climate performance and sensitivity to parametrized physics with emphasis on tropical convection. Clim Dyn 27(7–8):787–813

IPCC (2001) Climate change 2001, the scientific basis. Cambridge University press, Cambridge

Kalnay E, Kanamitsu M, Kistler R, Collins W, Deaven D, Gandin L, Iredell M, Saha S, White G, Woollen J, Zhu Y, Chelliah M, Ebisuzaki W, Higgins W, Janowiak J, Mo KC, Ropelewski C, Wang J, Leetmaa A, Reynolds R, Jenne R, Joseph D (1996) The NCEP/NCAR 40-year reanalysis project. Bull Am Meteorol Soc 77(3):437–471

Krinner G, Viovy N, de Noblet-Ducoudre N, Ogee J, Polcher J, Friedlingstein P, Ciais P, Sitch S, Prentice I (2005) A dynamic global vegetation model for studies of the coupled atmosphere–biosphere system. Global Biogeochem Cycles 19(1):GB1015

Latif M, Sperber K, Arblaster J, Braconnot P, Chen D, Colman A, Cubasch U, Cooper C, Delecluse P, DeWitt D, Fairhead L, Flato G, Hogan T, Ji M, Kimoto M, Kitoh A, Knutson T, Le Treut H, Li T, Manabe S, Marti O, Mechoso C, Meehl G, Power S, Roeckner E, Sirven J, Terray L, Vintzileos A, Voss R, Wang B, Washington W, Yoshikawa I, Yu J, Zebiak S (2001) ENSIP: the el nino simulation intercomparison project. Clim Dyn 18(3–4):255–276

Levitus S (1982) Climatological atlas of the world ocean. NOAA Professional paper, Washington

Li X (1999) Ensemble atmospheric gcm simulations of climate interannual variability from 1979 to 1994. J Clim 12:986–1001

Ma CC, Mechoso CR, Robertson AW, Arakawa A (1996) Peruvian stratus clouds and the tropical pacific circulation: a coupled ocean–atmosphere gcm study. J Clim 9(7):1635–1645

Madec G, Delecluse P, Imbart M, Levy C (1998) Opa 8.1 ocean general circulation model reference manual. Note du Pôle de modélisation, Institut Pierre-Simon Laplace 11:94 pp

Marti O, Braconnot P, Bellier J, Benshila R, Bony S, Brockmann P, Cadule P, Caubel A, Denvil S, Dufresne JL, Fairhead L, Filiberti MA, Foujols MA, Fichefet T, Friedlingstein P, Goosse H, Grandpeix JY, Hourdin F, Krinner G, Lévy C, Madec G, Musat I, deNoblet N, Polcher J, Talandier C (2005) The new IPSL climate system model:IPSL-CM4. Note du Pôle de Modélisation n 26, ISSN 1288–1619

Meehl GA, Washington WM, Arblaster JM, Hu AX (2004) Factors affecting climate sensitivity in global coupled models. J Clim 17(7):1584–1596

Menkes C, Boulanger JP, Busalacchi AJ, Vialard J, Delecluse P, McPhaden MJ, Hackert E, Grima N (1998) Impact of TAO vs. ERS wind stresses onto simulations of the tropical pacific ocean during the 1993–1998 period by OPA ogcm. Climatic impact of scale interactions for the tropical ocean–atmosphere system. Euroclivar Workshop Rep. 13, pp 46–48

Nigam S, Chao Y (1996) Evolution dynamics of tropical ocean–atmosphere annual cycle variability. J Clim 9(12):3187–3205

Pyatt HE, Albrecht BA, Fairall C, Hare JE, Bond N, Minnis P, Ayers JK (2005) Evolution of marine atmospheric boundary layer structure across the cold tongue–ITCZ complex. J Clim 18(5):737–753

Reynolds RW (1988) A real time global sea-surface temperature analysis. J Clim 1:75–86

Rossow WB, Schiffer RA (1999) Advances in understanding clouds from ISCCP. Bull Am Meteorol Soc 80(11):2261–2287

Swingedouw D, Braconnot P, Delecluse P, Guilyardi E, Marti O (2005) Sensitivity of the atlantic thermohaline circulation to global freshwater forcing. Clim Dyn. doi:101007/s00382-006-0171-3

Swingedouw D, Braconnot P, Marti O (2006) Sensitivity of the atlantic meridional overturning circulation to the melting from northern glaciers in climate change experiments. Geophys Res Lett 33(7):L07711

Terray L, Sevault E, Guilyardi E, Thual O (1995) The OASIS coupler user guide version 2.0. Cerfacs technical report TR/CMGC:95–46

Tiedtke M (1989) A comprehensive mass flux scheme for cumulus parameterization in large-scale models. Mon Weather Rev 117(8):1779–1800

Trenberth K, Salomon A (1994) The global heat balance: heat transports in the atmosphere and ocean. Clim Dyn 10:107–134

Uppala SM, Kållberg PW, Simmons AJ, Andrae U, da Costa Bechtold V, Fiorino M, Gibson JK, Haseler J, Hernandez A, Kelly GA, Li X, Onogi K, Saarinen S, Sokka N, Allan RP, Andersson E, Arpe K, Balmaseda MA, Beljaars ACM, van de Berg L, Bidlot J, Bormann N, Caires S, Chevallier F, Dethof A, Dragosavac M, Fisher M, Fuentes M, Hagemann S, Hólm E, Hoskins BJ, Isaksen L, Janssen PAEM, Jenne R, McNally AP, Mahfouf JF, Morcrette JJ, Rayner NA, Saunders RW, Simon P, Sterl A, Trenberth KE, Untch A, Vasiljevic D, Viterbo P, Woollen J (2005) The ERA-40 re-analysis. Quart J R Meteorol Soc 131:2961–3012. doi:10.1256/qj.04.176

Wang B (1994) On the annual cycle in the tropical eastern central pacific. J Clim 7(12):1926–1942

Xie P, Arkin P (1996) Analyses of global monthly precipitation using gauge observations, satellite estimates, and numerical model predictions. J Clim 9(4):840–858

Xie S, Saito K (2001) Formation and variability of a northerly ITCZ in a hybrid coupled AGCM: Continental forcing and oceanic–atmospheric feedback. J Clim 14(6):1262–1276

Yu JY, Mechoso CR (1999) Links between annual variations of peruvian stratocumulus clouds and of SST in the eastern equatorial pacific. J Clim 12(11):3305–3318